INFECTION AND IMMUNITY, Oct. 2009, p. 4265–4274 Vol. 77, No. 10
0019-9567/09/$08.00+0 doi:10.1128/IAI.00458-09

Complicated Urinary Tract Infection Is Associated with Uroepithelial Expression of Proinflammatory Protein S100A8▽†

Leticia Reyes,[1]* Sophie Alvarez,[2]‡ Ayman Allam,[1] Mary Reinhard,[1] and Mary B. Brown[1]

University of Florida, College of Veterinary Medicine, Department of Infectious Diseases and Pathology, P.O. Box 110880, Gainesville, Florida 32611-0880,[1] and Interdisciplinary Center for Biotechnology Research, University of Florida, Gainesville, Florida 32611[2]

Received 23 April 2009/Returned for modification 5 June 2009/Accepted 30 July 2009

F344 rats chronically infected with *Ureaplasma parvum* develop two distinct profiles: asymptomatic urinary tract infection (UTI) and UTI complicated by struvite urolithiasis. To identify factors that affect disease outcome, we characterized the temporal host immune response during infection by histopathologic analysis and in situ localization of *U. parvum*. We also used differential quantitative proteomics to identify distinguishing host cellular responses associated with complicated UTI. In animals in which microbial colonization was limited to the mucosal surface, inflammation was indistinguishable from that which occurred in sham-inoculated controls, and the inflammation resolved by 72 h postinoculation (p.i.) in both groups. However, inflammation persisted in animals with microbial colonization that extended into the deeper layers of the submucosa. Proteome profiling showed that bladder tissues from animals with complicated UTIs had significant increases ($P < 0.01$) in proteins involved in apoptosis, oxidative stress, and inflammation. Animals with complicated UTIs (2 weeks p.i.) had the highest concentrations of the proinflammatory protein S100A8 ($P \leq 0.005$) in bladder tissues, and the levels of S100A8 positively correlated with those of proinflammatory cytokines GRO/KC ($P \leq 0.003$) and interleukin-1α ($P \leq 0.03$) in urine. The bladder uroepithelium was a prominent cell source of S100A8-S100A9 in animals with complicated UTIs (2 weeks p.i.), which was not detected in animals with asymptomatic UTIs (2 weeks p.i.) or in any bladder tissues harvested at earlier p.i. time points. Based on these results, we surmise that invasive colonization of the bladder triggers chronic inflammation and immune dysregulation, which may be critical to struvite formation.

Struvite or infection stones form as a result of complicated urinary tract infections (UTI) caused by urease-producing bacteria such as *Proteus*, *Klebsiella*, *Serratia*, and *Ureaplasma* species (5, 8, 9, 17). Bacterial urease breaks down urea into ammonia, resulting in urine's becoming supersaturated with ammonia. When this occurs, the urine pH rises and the solubility of magnesium ammonium phosphate decreases, leading to crystal deposition and stone formation. Infection is always an underlying cause of struvite urolithiasis (5, 9). Therefore, it is not surprising that known predisposing factors such as renal tubular acidosis, neurogenic bladder, urinary tract obstructions, and chronic use of indwelling catheters (5, 9) are related to elements that increase patient susceptibility to UTI. Although infections usually induce an inflammatory response in the host, to our knowledge, the role of the host immune response as a potential predisposing factor in struvite urolithiasis has not been evaluated or considered to be important in disease pathogenesis. We present data suggesting that the host immune response plays a critical role in the development of struvite stones and that the proinflammatory protein S100A8–S100A9 may play a critical role in the chronic inflammation and immune dysregulation that ultimately result in struvite formation.

The genetically inbred Fischer (F344) rat is susceptible to UTI induced by the obligate urease producer *Ureaplasma parvum* (21). F344 rats experimentally inoculated with the same doses and strains of *U. parvum* develop two clinical profiles in response to infection: asymptomatic UTI and UTI complicated by chronic active inflammation and struvite stone formation. Asymptomatic UTI is characterized by a minimal immune response and the ascension of infection to the kidney. In contrast, rats with complicated UTI typically have elevated levels of proinflammatory cytokines such as interleukin-1α (IL-1α), IL-1β, IL-6, GRO/KC, and tumor necrosis factor alpha in their urine, and this condition is accompanied by edema, with areas of uroepithelial erosion and/or proliferation, and extensive leukocyte infiltration into the renal pelvis and bladder. The initial dose of *U. parvum* does not seem to influence which clinical profile of UTI develops but does determine if an animal is successfully colonized by the microbe (20). In order to identify factors that affect disease outcome, we characterized the temporal host immune response during infection by histopathologic analysis and in situ localization of *U. parvum*. We also used differential quantitative proteomics to identify distinguishing host cellular responses associated with complicated UTI.

MATERIALS AND METHODS

Sample selection and protein extraction for rat bladder proteome studies. Archived bladder tissues obtained from F344 rats in a previous study were used for these experiments (20). All procedures were performed in accordance with the guidelines of the Institutional Animal Care and Use Committee. Sterile 10B

* Corresponding author. Mailing address: University of Florida, College of Veterinary Medicine, Department of Infectious Diseases & Pathology, P.O. Box 110880, Gainesville, FL 32611-0880. Phone: (352) 294-4090, ext. 3990. Fax: (352) 846-2781. E-mail: lreyes@ufl.edu.

† Supplemental material for this article may be found at http://iai.asm.org/.

‡ Present address: Donald Danforth Plant Science Center, 975 N. Warson Rd., St. Louis, MO 63132.

▽ Published ahead of print on 10 August 2009.

broth or a rat-adapted strain of *U. parvum* (21) was inoculated directly into the bladders of rats, and tissues were harvested at 1, 2, and 3 days and 2 weeks postinoculation (p.i.). Tissues were cultured for the presence of *U. parvum*, and bladders were evaluated by histopathologic analyses. For proteome studies, animals infected for 2 weeks and the corresponding bladder tissues were assigned to the asymptomatic UTI or struvite group based on culture status, the urine cytokine profile, histology, and the presence of struvite uroliths (21). Animals within the UTI group were culture positive at the time of necropsy and had minimal histologic lesions, low urine cytokine levels, and no evidence of struvite uroliths. Animals within the struvite group were culture positive at the time of necropsy, had extensive histologic changes in bladder tissues, were positive for struvites, and had marked elevations in urine proinflammatory cytokine levels. In order to minimize the variability of the *U. parvum* protein load between groups, only tissues that had similar log numbers of CFU (2.4 to 2.7) at the time of necropsy were chosen for these experiments. Protein from tissues was extracted with Trizol according to the protocol of the manufacturer (Invitrogen Corp., Carlsbad, CA). Pelleted protein extracts were allowed to air dry and stored at −20°C before analysis.

Quantitative proteomics using peptide labeling and two-dimensional (2D) liquid chromatography-tandem mass spectrometry (LC-MS/MS). Protein extracts from two rats in the asymptomatic UTI group and two rats in the struvite group were prepared. Rat bladder protein extracts were processed and labeled with the amine-specific peptide-based labeling system iTRAQ according to the instructions of the manufacturer (Applied Biosystems, Foster City, CA). Briefly, a 60-μg aliquot of each sample was dissolved in 20 μl of dissolution buffer (0.5 M triethylammonium bicarbonate) and reduced with reducing agent (50 mM Tris-2-carboxyethyl phosphine) at 60°C for 1 h. After reduction, cysteines were blocked with 200 mM methyl methanethiosulfonate for 10 min at room temperature. Ten microliters of a trypsin solution (Promega Corporation, Madison, WI) was added to each sample, and samples were incubated overnight at 37°C. After digestion, bladder protein extracts from the asymptomatic UTI group were labeled with reagent 116 and bladder protein extracts from the struvite group were labeled with reagent 117. One sample from the asymptomatic UTI group and one sample from the struvite group were combined. Two biological replicates were processed in the same way. Pooled samples were desalted by using a macrospin Vyadac silica C_{18} column (The Nest Group Inc., Southboro, MA) prior to the strong cation exchange procedure.

Strong cation exchange fractionation of desalted iTRAQ-labeled peptides was performed with a PolySULFOETHYL A column (length by internal diameter, 100 by 2.1 mm; particle size, 5 μm; pore size, 300 Å). Peptides resuspended in buffer A (75% 0.01 M ammonium formate, 25% ACN) were eluted over a linear gradient of 0 to 20% buffer B (75% 0.5 M ammonium formate, 25% ACN) and detected at an absorbance of 280 nm. Eluted fractions were further separated by capillary reverse-phase high-performance LC using an LC Packings C_{18} PepMap column (DIONEX, Sunnyvale, CA). Mass spectrometric analysis of the column eluate was performed in-line with a QSTAR hybrid quadrupole time of flight mass spectrometer (Applied Biosystems Inc.). The focusing potential and ion spray voltage were set to 275 V and 2,600 V, respectively. The information-dependent acquisition mode of operation was employed for the acquisition of a survey scan from *m/z* 400 to 1,200, followed by collision-induced dissociation of the three most intense ions.

Tandem mass spectra were extracted by Analyst (v 1.1.; Applied Biosystems Inc.). The International Protein Index rat database v 3.32 (12) (concatenation of the forward and random sequences) was used for protein identification. Searches were performed using MS/MS data interpretation algorithms from Protein Pilot (Paragon algorithm, v 2.0; Applied Biosystems Inc.) and Mascot (v 2.2; Matrix Science, London, United Kingdom). The Paragon algorithm from Protein Pilot was set up to search iTRAQ 4-plex samples as variable modifications with methyl methanethiosulfonate as a fixed modification. The Protein Pilot algorithm was selected to search automatically for biological modifications such as the presence of homocysteines. Additional information on this algorithm is found in reference 23. The confidence level for protein identification was set up to 1.3 (95%), which is the default for the detected protein threshold in the Paragon method. A false-discovery rate was calculated at 0.4% as the percentage of progroups which matched randomized accessions in the concatenated database. The differential expression ratios for protein quantitation were obtained from Protein Pilot, which calculates protein ratios using only ratios from the spectra that are distinctive to each protein, excluding the shared peptides of protein isoforms. Peptides with low spectral counts were also excluded from the calculation of averages by setting the intensity threshold for the sum of the signal-to-noise ratios for all the peak pairs at >9. All the quantitative ratios were then corrected for bias automatically by Protein Pilot when the data were processed to create the Pro Group algorithm results. The bias factor calculated for the iTRAQ reagent 116/ reagent 117 ratio was 0.93. Each protein that was quantified was identified by a minimum of three spectra, with an error factor of <2. The error factor is a measure of the variation among the different iTRAQ ratios (the greater the variation, the greater the uncertainty) and represents the 95% uncertainty range for a reported ratio. The *P* value is calculated based on the 95% confidence interval.

Proteome profiling of bladder tissues by 2D differential gel electrophoresis. Protein extracts from five rats in the asymptomatic UTI group and three rats in the struvite group were used for 2D gel electrophoresis. Protein pellets were dissolved in buffer containing 8 M urea, 2 M thiourea, 4% CHAPS {3-[(3-cholamidopropyl)-dimethylammonio]-1-propanesulfonate}, and 10 mM Tris, pH 8.5. The total protein content of each sample was determined by the Lowry assay. Samples from each group of animals contained pooled protein extracts from three biological replicates, and the concentration of protein pools was adjusted so that the samples from the two groups contained the same total concentrations. Protein from the bladders of struvite-positive rats was labeled with Cy5 fluorescent dye, and protein from the bladders of struvite-negative rats was labeled with Cy3 fluorescent dye. Aliquots of 50 μg from each sample were mixed, and isoelectric focusing was done with a pH 3 to 11 immobilized pH gradient strip exposed to 8,000 V for 54.5 kV · h. Separation by molecular weight was done with an 8 to 16% Tris-glycine sodium dodecyl sulfate-polyacrylamide gel.

Protein spots within the gel were scanned with a Typhoon 8600 variable-mode imager (Amersham Biosciences, Piscataway, NJ). Data processing and spot quantification were performed with Phoretix software (Nonlinear USA Inc., Durham, NC). Filtering of background noise and normalization of the gel image were performed prior to analysis. A reference value (normalized volume) was created for each spot on the gel.

Protein spots unique to either treatment group were manually excised from the gel for identification by mass spectrometry. For each spot, a corresponding negative control was created that consisted of an equivalent-size gel that stained negative for protein with Coomassie blue. Protein destaining and enzymatic digestion were performed as described previously (27). Briefly, gel spots were destained, washed in 50% acetonitrile in 25 mM ammonium bicarbonate buffer, and dehydrated in a SpeedVac centrifuge for 15 min. Protein was reduced and alkylated by incubation with 45 mM dithiothreitol for 30 min at room temperature followed by incubation with 100 mM iodoacetamide for 30 min in darkness. Gel pieces were then washed in 50% acetonitrile in 50 mM ammonium bicarbonate and dehydrated in the SpeedVac for 15 min prior to digestion with a trypsin enzyme cocktail (12.5 ng/μl of trypsin in 50 mM ammonium bicarbonate, pH 8.4, 5 mM $CaCl_2$). The enzyme cocktail was added to the sample at a ratio of 1:20, enzyme to protein.

Digested protein samples extracted from the gel were separated and identified using LC-MS/MS as described above for the iTRAQ fractions. MS/MS data were compared against the NCBInr sequence database by using the Mascot (Matrix Science, Boston, MA) database search engine. Peptide sequences with probability-based molecular weight search scores above the default significance value ($P < 0.05$) were used for protein identification. All protein identifications were validated by manual inspection of the MS/MS data.

Detection of S100A8 in urine and bladder tissues by ELISA. A minimum of five bladder tissue samples each from sham-inoculated controls, infected struvite-negative animals, and infected struvite-positive animals were selected for detection of S100A8 protein by capture enzyme-linked immunosorbent assay (ELISA). Bladder tissue samples were homogenized in cold sterile saline and stored frozen at −80°C until use. The OptEIA ELISA reagent kit B (BD Biosciences, San Diego, CA) was used to perform the assay. Mouse monoclonal anticalprotectin, ab50143 (Abcam Inc., Cambridge, MA), was used as the capture antibody at a concentration of 5 μg/ml. Wells designated negative controls were incubated with plain diluent buffer. Wells designated positive controls were loaded with homogenized rat spleen tissue. Samples were loaded onto ELISA plates in duplicate, and the plates were incubated for 18 h at 4°C. Biotin-conjugated anti-mouse S100A8 (R & D Systems, Minneapolis, MN) was prepared at a concentration of 0.2 μg/ml, and ELISA plates were incubated at 37°C for 4 h. Avidin-horseradish peroxidase conjugate was used at a dilution of 1:1,000 and applied to each well for 30 min. After the plates were washed, 3,3′,5,5′-tetramethylbenzidine (TMB) substrate (BD Biosciences) was used to measure horseradish peroxidase activity, and the substrate reaction was stopped with BD OptEIA stop solution. Absorbance values were measured at a 450-nm wavelength with an ELx808 ultra-microplate reader (Bio-Tek Instruments, Inc., Winooski, VT).

For normalization purposes, the total protein concentration in each sample was determined by using a micro-bicinchoninic acid protein assay kit (Pierce Chemicals, Rockwood, MD). Absorbance values obtained by ELISA were di-

vided by the total protein concentration so that values are reported as the absorbance value per microgram.

Immunohistochemical detection of *U. parvum* and the heterodimer complex S100A8-S100A9 in bladder tissue. Primary antibodies were anti-*U. parvum* rabbit polyclonal antibody (a gift from Janet Robertson, Medical Microbiology and Immunology, University of Alberta), anti-S100A8-S100A9 mouse monoclonal MAC387 (Thermo Scientific, Fremont, CA), and mouse immunoglobulin G (IgG) clone NCG01 and rabbit IgG isotype controls (Thermo Scientific, Fremont, CA). MAC387 antibody recognizes the S100A8-S100A9 heterodimer complex (7). Secondary antibodies were Alexa Fluor-660 goat anti-mouse IgG and Alexa Fluor-594 (Invitrogen Corp., Carlsbad, CA). Nuclei were stained with DAPI (4′,6-diamidino-2-phenylindole) or Sytox (Invitrogen Corp., Carlsbad, CA).

Five-micrometer-thick sections were made from archived paraffin-embedded periodate-lysine-paraformaldehyde-fixed bladder tissues (33). Tissues were deparaffinized through a series of washes: two washes in xylene, followed by a series of graded ethanol (100, 95, 75, and 50%) washes of 10 min each. Slides soaked in 50% ethanol were allowed to equilibrate in phosphate-buffered saline (PBS) for 10 min. For antigen retrieval, tissues were incubated in 1% trypsin for 5 min at room temperature, washed in PBS, and permeabilized with 0.1% Triton X for 3 min at room temperature. After being washed in PBS, tissue sections were incubated in a blocking solution (2% goat serum, 1% bovine serum albumin, 0.1% Triton X-100, 0.05% Tween 20, and 0.05% sodium azide in 0.01 M PBS) for 30 min at room temperature. Tissue sections were incubated overnight at 4°C with primary antibodies diluted 1:200 in blocking buffer. After being washed with PBS, tissue sections were treated with Image-iT FX signal enhancer (Invitrogen Corp., Carlsbad, CA) for 30 min and washed again with PBS. Microscope slides were then incubated with the secondary antibody, diluted 1:2,000 in blocking buffer, for 30 min at room temperature. After the slides were washed, nuclei were stained with Sytox green (1 μM concentration) or DAPI. Unbound Sytox green was removed by washing slides in 0.9% saline. Slides were air dried, and coverslips were secured with ProLong Gold mounting reagent (Invitrogen Corp., Carlsbad, CA).

Confocal microscopy. Images were captured with an Olympus IX81-DSU spinning-disk confocal microscope using Slidebook software (Olympus, Center Valley, PA). During image capture, camera settings were optimized using the tissue section with the highest degree of fluorescent signaling. Once the image capture settings were established, the same settings were used for all the tissues within the specific labeling experiment.

Statistical data analysis. Data from multiple experiments were grouped together in order to make statistical analysis possible. Data were analyzed by one-way analysis of variance (ANOVA). Fisher's multiple-comparison test was used when the ANOVA indicated a significant difference among group means. Regression analysis was used to determine if there was a correlation between S100A8 and urine cytokine concentrations. For all analyses, a probability P of ≤ 0.05 was considered significant.

RESULTS

Inflammatory response to *U. parvum* is influenced by the location of the organism in bladder tissue. The inflammatory responses of sham-inoculated control animals and of animals inoculated with *U. parvum* were indistinguishable until 48 h p.i. The early immune response (before 48 h) consisted of various degrees of uroepithelial desquamation with hemorrhaging, edema, and leukocyte infiltration. The infiltrating leukocytes consisted of neutrophils, macrophages, and lymphocytes (data not shown). At 48 h p.i., inflammatory lesions in sham-inoculated controls were resolving. The uroepithelium was mostly intact, hemorrhaging had stopped, and any leukocytes that were present were mononuclear (data not shown). Infected animals showed various degrees of inflammation. In some animals, the inflammation was restricted to small, scant areas within the superficial layers of the submucosa (data not shown). In others, it continued to be extensive and involved the muscularis layers as well as the submucosa and uroepithelium. By 72 h, all sham-inoculated controls had resolved inflammation (Fig. 1A). At 72 h p.i., there was a marked divergence in the inflammatory responses in infected animals. Fifty percent of animals showed resolution of inflammation, which was characterized by an intact uroepithelium, a normal muscularis layer, and scant foci of submucosal edema, at 72 h p.i. (Fig. 1B). The few leukocytes that could be identified were predominantly mononuclear. Active inflammation, characterized by multiple foci of uroepithelial erosion and extensive edema of the submucosa, was observed in the remaining 50% of infected animals at 72 h p.i. An interesting feature in the animals with active inflammation was the influx of eosinophils intermixed with neutrophils into the edematous tissue. In these animals, necrosis and proliferation of fibroblasts occurred in the deep submucosa and penetrated into the muscularis layer of the bladder (Fig. 1C). Similarly, animals with complicated UTI also showed infiltration of eosinophils intermixed with neutrophils and fibroblast proliferation in the submucosa of the bladder (Fig. 2C).

In situ detection of *U. parvum* in tissue sections harvested from animals infected for 72 h also showed divergent patterns of tissue colonization. In animals with resolving inflammation, *U. parvum* was found primarily attached to the uroepithelium and concentrated along the luminal surface of the mucosa (Fig. 1E). Animals with active inflammation also had colonization of the mucosal surface. However, in these animals, *U. parvum* was also found to be associated with white cells and fibroblasts within the edematous areas in the submucosal layer of the bladder (Fig. 1F). *U. parvum* was not detected in the muscularis layers in any of the infected animals.

U. parvum could also be identified in the bladder tissues of animals at 2 weeks p.i. (Fig. 2). Animals with asymptomatic UTI and animals with resolving inflammation showed similar patterns of colonization. In both these groups, *U. parvum* was identified primarily in the uroepithelial layer (Fig. 2E). Some organisms could also be found in the superficial layers of the submucosa, but there was no evidence of inflammation at these sites of colonization. Animals with complicated UTI also showed microbial colonization within the hyperplastic uroepithelium without leukocyte infiltration (data not shown). However, in these animals, *U. parvum* was also located within active sites of inflammation that were present in the deep layers of the submucosa (Fig. 2F).

Proteomics approaches show that uroepithelial biological processes in animals with struvites markedly differ from those in animals with asymptomatic UTI. Reverse-phase LC-MS/MS analyses of rat bladder tissues identified 336 proteins with 95% confidence. Protein lists can be viewed in Tables S1 to S3 in the supplemental material. One hundred ten proteins were present in significantly higher concentrations in animals with complicated UTI/struvites (see Table S1 in the supplemental material) than in animals with asymptomatic UTI, while 108 proteins were present in significantly higher concentrations in animals with asymptomatic UTI (see Table S2 in the supplemental material). One hundred eighteen proteins were found to have equivalent concentrations in the two clinical groups (see Table S3 in the supplemental material). Figure 3 shows the frequency distribution of proteins that significantly differed in concentration or were equivalent among the clinical profiles. Gene ontology information was used to group proteins according to their general biological function. Animals with struvites had a unique emphasis on proteins that are upregulated during stress (Fig. 3A), for example, 10-kDa heat shock

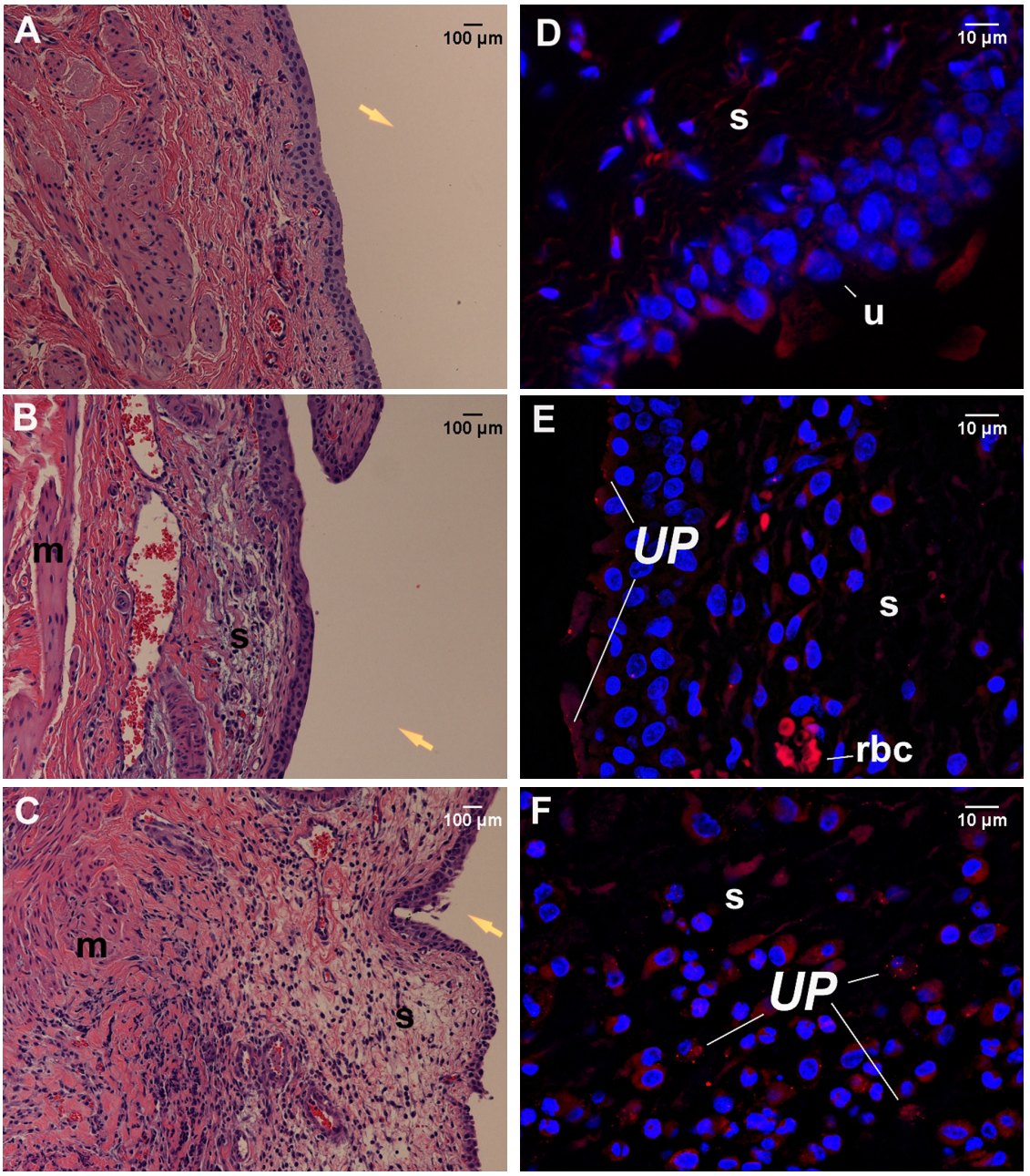

FIG. 1. Histopathologic profiles and in situ location of *U. parvum* in the bladder tissues of F344 rats experimentally infected for 72 h. (A to C) Images of hematoxylin-eosin-stained sections of bladder tissues from control animals (A), infected animals with resolving inflammation (B), and infected animals with active inflammation (C) were taken at a magnification of ×200. The yellow arrows are placed in the area that would represent the bladder lumen. (D to F) Immunofluorescent images of isotype control tissues (D) and tissues from infected animals with resolving inflammation (E) and infected animals with active inflammation (F) were taken at a magnification of ×600; images are 2D projections of image stacks. *U. parvum* (*UP*) was labeled with Alexa Fluor-594 (red), and nuclei were stained with DAPI (blue). Panel D shows a *U. parvum*-positive bladder section stained with isotype antibody, therefore demonstrating the degrees of nonspecific binding and tissue autofluorescence. s, submucosa; u, uroepithelium; rbc, red blood cell.

protein, α-crystallin β-chain, peroxiredoxins 5 and 6, glutathione peroxidase 3, and carbonic anhydrase 3. Rats with struvites also showed a significant emphasis on proteins that regulate apoptosis, such as PYCARD apoptosis-associated speck-like protein, annexin A1, mitochondrial fission 1 protein, heat shock protein beta-1, isoform 4 of reticulon-4, and cystatin B. These animals also exhibited a significant shift toward mitochondrial metabolic processes that constitute the electron transport system and the proton transport system, which was not evident in the asymptomatic UTI group (see Table S1 in the supplemental material).

Animals in the asymptomatic UTI group showed significant increases in proteins that regulate cell adhesion, maintain tight cell junctions, and maintain the extracellular matrix (Fig. 3B; see also Table S2 in the supplemental material). This group

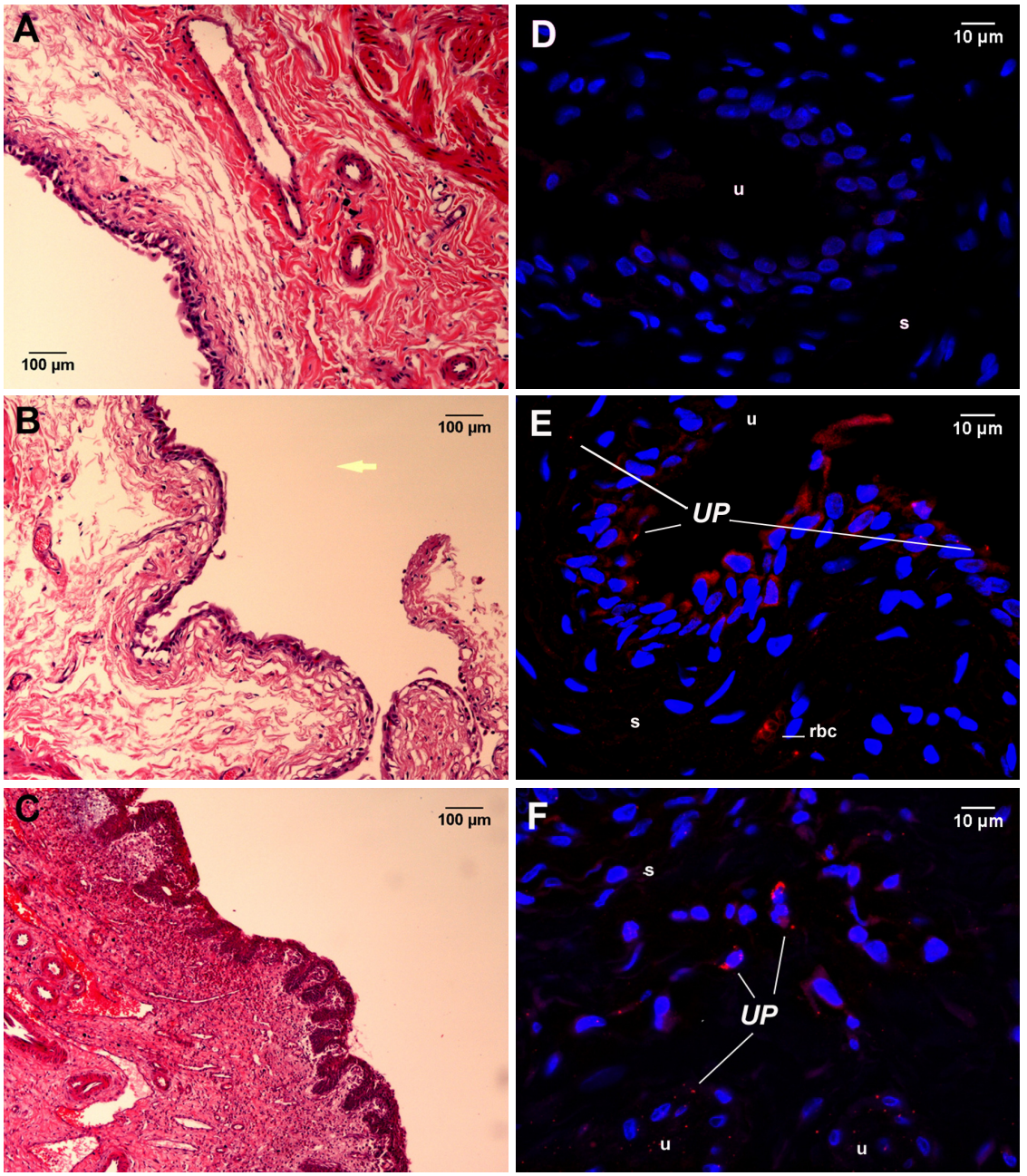

FIG. 2. Histopathologic profiles and in situ location of *U. parvum* in the bladder tissues of F344 rats experimentally infected for 2 weeks. (A to C) Images of hematoxylin-eosin-stained sections of bladder tissues from control animals (A) and animals with asymptomatic UTI (B) and complicated UTI (C) were taken at a magnification of ×200. The yellow arrow is placed in the area that would represent the bladder lumen. (D to F) Immunofluorescent images of tissues from uninfected control animals (D) and animals with asymptomatic UTI (E) and complicated UTI (F) were taken at a magnification of ×600; images are 2D projections of image stacks. *U. parvum* (*UP*) was labeled with Alexa Fluor-594 (red), and nuclei were stained with DAPI (blue). Panel D shows a *U. parvum*-positive bladder section stained with isotype antibody, therefore demonstrating the degrees of nonspecific binding and tissue autofluorescence. s, submucosa; u, uroepithelium; rbc, red blood cell.

also showed a greater concentration of proteins that regulate and maintain the cell cytoskeleton and cytoskeleton-dependent functions. Unlike the struvite group, these animals exhibited an increase in enzymes that regulate carbohydrate metabolism.

There were qualitative differences in the profiles of proteins that were grouped into the inflammation and immunity category. For example, the struvite group had significant increases in proinflammatory proteins such as S100A8, S100A9, galectin-3, c-type lectin, and macrophage inhibitory protein. Proteins that participate in antigen presentation (β2-microglobulin and Psme 1) were also significantly increased in struvite-positive animals. Animals in the asymptomatic UTI group did not display a panel of proteins that convey a distinct immune function (see Table S2 in the supplemental material).

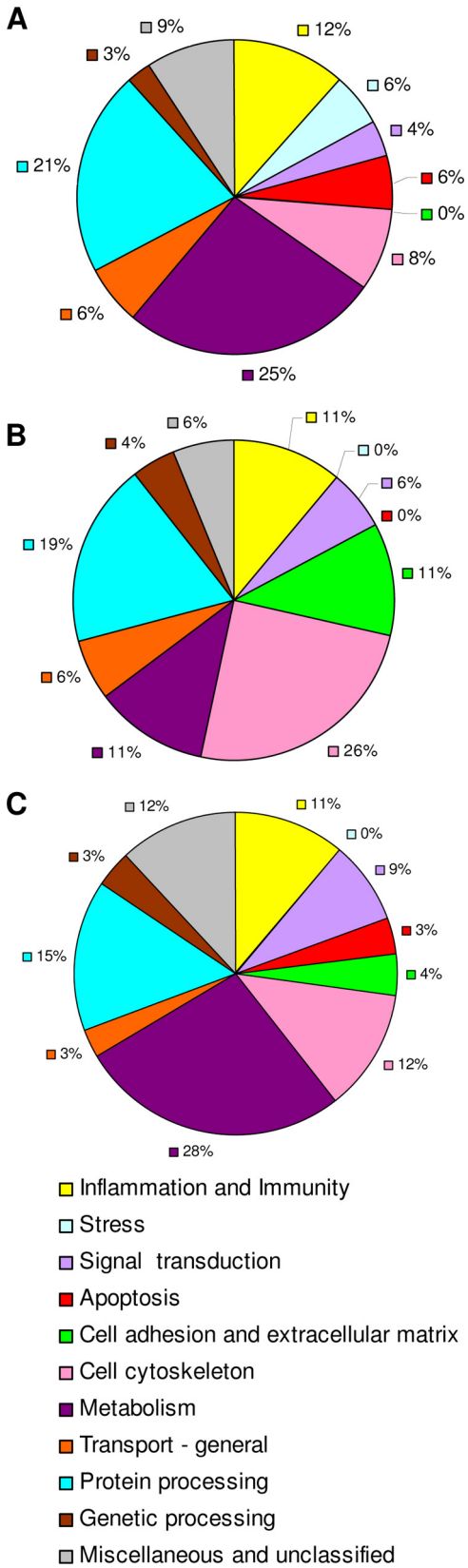

FIG. 3. Overall biological activity in bladder tissues of animals with UTI. Values are percentages of proteins within each biological function group according to gene ontology designations for each protein as listed in the Rat Genome Database or the PANTHER classification database. Proteins were identified and relative concentrations were determined by using the Pro Group algorithm. Graph A shows the percent distribution of proteins with significantly greater levels in animals with complicated UTI than in animals with asymptomatic UTI ($P < 0.01$). Graph B shows the percent distribution of proteins with significantly greater levels in animals with asymptomatic UTI ($P < 0.01$), and graph C shows the percent distribution of proteins that were equivalent among animals in the two groups.

Most of the proteins that were elevated in this group (apolipoprotein H, plasminogen precursor, C9 protein, and α-2-HS-glycoprotein precursor) may actually be the by-products of immune activation or of inflammation instead of modulators of that activity.

S100A8 concentrations in bladder tissues correlate with urinary IL-1α and GRO/KC. Quantitative proteomics using iTRAQ analysis showed elevated ratios of protein concentrations (those in the struvite group to those in the asymptomatic UTI group) of 8.7199 for S100A8 and 8.9710 for S100A9 (see Table S2 in the supplemental material). Differential 2D gel electrophoresis showed a similar pattern in that S100A8 could be detected in animals with struvites but not in animals in the asymptomatic UTI group (see Table S4 in the supplemental material).

In order to correlate urine cytokine concentrations with S100A8, an ELISA method was developed. Sham-inoculated control animals were included in this analysis. The detection of S100A8 in urine was inconsistent in that it did not correlate with levels obtained in bladder homogenates (data not shown). Only animals in the struvite group had detectable S100A8 in their urine; however, not all animals with elevated levels of S100A8 in bladder tissue homogenates had concomitant detectable levels of this protein in their urine. Regardless, the animals with detectable levels of S100A8 in urine had the most pronounced inflammatory lesions in their bladder tissues. Figure 4A shows concentrations of S100A8 in the bladder tissue homogenates from control and infected animals. Animals in the struvite group had significantly higher concentrations of S100A8 than animals in the control group ($P < 0.005$) and the asymptomatic UTI group ($P < 0.0001$). There was a significant positive correlation between the amount of S100A8 present in bladder tissue homogenates and the concentrations of GRO/KC and IL-1α in urine (Fig. 4B).

Animals with complicated UTI exhibit uroepithelial expression of S100A8-S100A9. In animal tissues obtained at 48 and 72 h and 2 weeks p.i., S100A8-S100A9 was detected only in the cytoplasm of neutrophils that were infiltrating the bladder tissues from animals exhibiting inflammation (data not shown). The bladder tissues from animals infected for 2 weeks showed a unique pattern of S100A8-S100A9 expression. The heterodimer complex was not detected in animals with asymptomatic UTI (Fig. 5C), which is not surprising since these animals were no longer exhibiting an inflammatory response. However, animals with complicated UTI showed extensive expression of S100A8-S100A9 in the uroepithelium (Fig. 5E) and endothelium within the submucosal layer of the bladder (Fig. 5G).

A

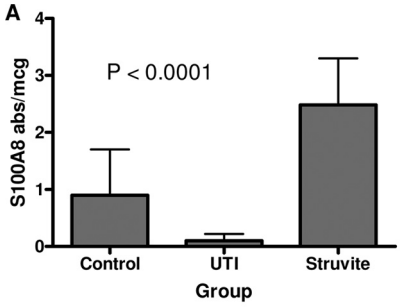

B

	Pearson correlation value to S100A8		
Cytokine	R	R^2	P value
GRO/KC	0.74	0.51	0.003
IL-1α	0.589	0.347	0.03
IL-1β	0.341	0.043	0.23

FIG. 4. Concentrations of S100A8 in bladder tissue homogenates from F344 rats. Values in panel A are mean S100A8 concentrations ± standard deviations, expressed as the absorbance value (abs) obtained by ELISA divided by the total protein concentration in micrograms. The *P* value listed in the graph was obtained by ANOVA ($n = 5$ for all groups). Animals in the struvite group had significantly higher concentrations of S100A8 than other animals, as determined by Fisher's protected least significant difference test ($P \leq 0.005$). Pearson correlation values for S100A8 concentrations in bladder tissue homogenates (absorbance value per microgram of total protein) and the corresponding urine cytokine concentrations are listed in panel B. Urine and bladder tissues were collected at the same time point, at 2 weeks p.i.

DISCUSSION

The uroepithelium plays a primary role in innate defense against microbial invasion. Under normal conditions, the bladder epithelium is quiescent, with low cell turnover (10, 25). Following exposure to bacteria, the uroepithelium shifts from a quiescent state to active production of proinflammatory cytokines/chemokines such as IL-1, IL-8, and tumor necrosis factor alpha. The cells also undergo necrosis or apoptosis and slough off from the basement membrane as a means of eradicating bacteria from the urinary tract (14). In response to uroepithelial signaling, neutrophils invade bladder tissue within 1 to 4 h of the initiating event and begin secreting proinflammatory cytokines, chemokines, and proteases (11) to kill the invading pathogen. This proinflammatory response can also damage the surrounding tissue, including the muscularis layer of the bladder (6). As the immune response progresses, invading macrophages engulf degraded cellular components and secrete IL-1 inhibitors, which reduce inflammation and facilitate the return to homeostasis (11). As bacteria are killed and removed, the remaining uroepithelium proliferates until the mucosal barrier is restored, at which time the uroepithelium reverts to a well-differentiated quiescent phenotype.

In our study, sham-inoculated controls showed an initial inflammatory response profile that was similar to that which occurred during infection and early UTI. The initial responses of all animals were characterized by uroepithelial desquamation, hemorrhage, edema, and leukocyte infiltration. In the sham-inoculated controls, these lesions completely resolved by 72 h p.i. Since these animals were confirmed to be free of infection at the time of necropsy, we can only conclude that the lesions were caused by the trauma of the inoculation procedure.

Infected animals with microbial colonization limited to the uroepithelium responded similarly to sham-inoculated controls in that bladder inflammation was nearly resolved by 72 h p.i., despite active bacterial colonization. This finding would suggest that the inflammatory events that occurred in the early phase of infection in these animals may actually have been triggered by the traumatic procedure rather than *U. parvum*. In animals with persistent inflammation at 72 h p.i., the distinguishing features were the extensive involvement of the submucosa and muscularis layers and the presence of eosinophils within sites of edema. Interestingly, the uroepithelial barrier in this group of animals was almost restored despite the edema and leukocyte infiltration that were still present in the deeper tissue layers of the bladder.

Animals with complicated UTI (infected for 2 weeks) had an inflammatory profile similar to that of animals with persistent inflammation at 72 h p.i. In both groups, *U. parvum* was located in the submucosal sites, with edema and leukocyte infiltration. Further, we could identify aggregates of *U. parvum* attached to submucosal fibroblasts in animals with complicated UTI. Therefore, we suggest that the interaction between *U. parvum* and cells such as fibroblasts and eosinophils that reside within the deeper tissues may be the trigger that leads to chronic active inflammation and a disease phenotype. In vitro studies have confirmed that ureaplasmas can directly induce IL-6 and IL-8 secretion in human pulmonary fibroblasts (26), thus providing support for this argument.

Pairwise proteome profiling of bladder tissues showed that animals with complicated UTI had evidence of oxidative stress as well as an increase in various proteins, including S100A8, that are involved in immune regulation. We focused our attention on S100A8 because of its pleiotropic effects on immune regulation (13, 15, 28). Neutrophil functions such as chemotaxis and induction of the respiratory burst are dependent on S100A8 (22). In addition to having potent chemotactic ability for granulocytes, S100A8 can potentiate cytokine expression through NF-κβ activation and nitric oxide production, which in turn increases cellular oxidative stress and the extent of tissue damage (3, 18). On the other hand, S100A8-S100A9 can also downregulate immune responses by inhibiting immunoglobulin production by lymphocytes and by inducing apoptosis of cells that regulate the inflammatory cascade (31, 34). Therefore, it was not surprising that animals with complicated UTI had significant increases in S100A8 and S100A9 expression, given the degree of neutrophilic infiltration into bladder tissues. The expression of S100A8-S100A9 by endothelial cells present within inflammatory foci (32) was also predictable. However, the predominant expression of S100A8-S100A9 by uroepithelial cells was an unexpected finding. Typically, these cells do not express this heterodimer complex, and its presence in the uroepithelium is normally considered to be a biomarker of immune dysregulation or neoplastic transformation (29, 30). We did not detect S100A8-S100A9 expression in the uroepithelia of animals from 48 and 72 h p.i., but neutrophils were positive for S100A8-S100A9, which confirmed the efficacy of the assay. Therefore, the induction of S100A8-S100A9 in the uroepithelia of animals with complicated UTI was a late event in the disease process. Further, induction of S100A8-S100A9 is likely not to be a direct effect of *U. parvum* colonization, since not all infected animals showed uroepithelial expression of

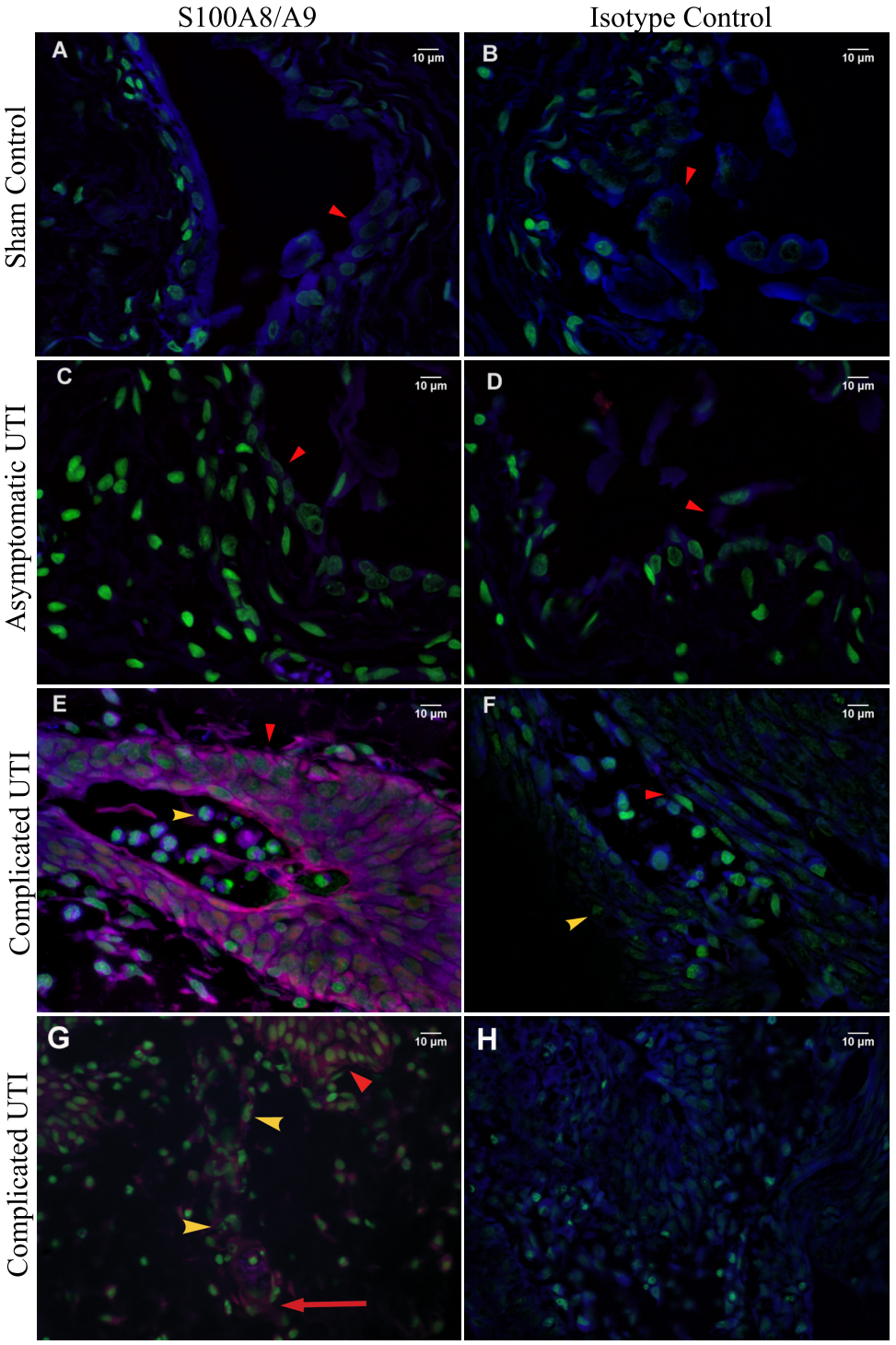

FIG. 5. Immunohistochemical detection of S100A8-S100A9 in the bladder tissues of F344 rats. Representative bladder tissue sections from control animals (A and B), animals with asymptomatic UTI (C and D), and animals in the struvite group (E to H) are shown. Images in panels A to F were taken at a magnification of ×600. Images in panels G and H were taken at a magnification of ×400. S100A8-S100A9 is labeled red, and nuclei are labeled green. Red arrowheads are pointing to the uroepithelium. Yellow arrowheads are pointing to neutrophils, and the long red arrow in panel G is pointing to endothelial cells expressing S100A8.

S100A8-S100A9. Instead, the expression of S100A8-S100A9 in animals with complicated UTI was more likely driven by a paracrine cytokine loop involving IL-1 and GRO/KC (13). IL-1α is known to induce the expression of S100A8 and S100A9 in epithelial cells (2, 19), and in turn, S100A8-S100A9 can induce the expression of GRO-α and GRO-β (32). We saw a positive correlation between S100A8 and GRO/KC in urine and a weaker association between S100A8 and IL-1α in urine

from animals with UTI. These findings provide additional support for a paracrine cytokine loop driving S100A8 and S100A9 expression in the bladder uroepithelium.

The results of our study provide new insights into the pathogenesis of struvite (magnesium ammonium phosphate) urolithiasis. To date, there are no published reports of studies examining the inflammatory response in struvite producers, despite the fact that UTI is considered a predisposing factor in struvite production (5, 9, 17). The current dogma only acknowledges the role of urease-producing bacteria in altering urine composition (5, 9). Specifically, urease from bacteria supersaturates urine with ammonia, which promotes magnesium ammonium phosphate crystallization in urine. Typically, struvite stones can develop as early as 4 to 6 six weeks after the initiating UTI. Although UTI typically induce a host inflammatory response, this aspect has never been considered to be important in disease pathogenesis. Ironically, since S100A8 is a principle component of the struvite stone matrix, it was thought that it may have a protective role by inhibiting calculogenesis (1, 4). Its role as a biomarker of chronic inflammation or immune dysregulation was not considered.

In our studies, genetically inbred F344 rats that were exposed to the same strains, culture stocks, and concentrations of *U. parvum* developed two distinct profiles: asymptomatic UTI or complicated UTI with struvite formation. Although we did not assess urine pH at the time of collection, it is reasonable to assume that urine supersaturation with ammonia occurred in all animals with UTI since *U. parvum* uses urease to produce 95% of its ATP (16, 24). Further, the organism could be located in the mucosal surface in all infected animals, thereby demonstrating ample opportunity for *U. parvum* to alter the ammonia concentration of the urine. The only distinctive feature differentiating the infection outcomes was the presence of chronic active inflammation in animals with UTI. The development of active inflammation preceded the expression of S100A8-S100A9 by the uroepithelium and the production of stones by 2 weeks. We suggest that a similar phenomenon may be occurring in humans, since struvite calculi also develop several weeks after the initial UTI event. Based on the results of these studies, the host immune response is a critical component in the pathogenesis of struvite urolithiasis.

ACKNOWLEDGMENTS

The project described herein was supported by award number K08DK075651 from the National Institute of Diabetes and Digestive and Kidney Diseases (NIDDK).

The content is solely the responsibility of the authors and does not necessarily represent the official views of the NIDDK or the National Institutes of Health.

REFERENCES

1. **Asakura, H., J. D. Selengut, W. H. Orme-Johnson, and S. P. Dretler.** 1998. The effect of calprotectin on the nucleation and growth of struvite crystals as assayed by light microscopy in real-time. J. Urol. **159:**1384–1389.
2. **Bando, M., Y. Hiroshima, M. Kataoka, Y. Shinohara, M. C. Herzberg, K. F. Ross, T. Nagata, and J. Kido.** 2007. Interleukin-1α regulates antimicrobial peptide expression in human keratinocytes. Immunol. Cell Biol. **85:**532–537.
3. **Benedyk, M., C. Sopalla, W. Nacken, G. Bode, H. Melkonyan, B. Banfi, and C. Kerkhoff.** 2007. HaCaT keratinocytes overexpressing the S100 proteins S100A8 and S100A9 show increased NADPH oxidase and NF-κB activities. J. Investig. Dermatol. **127:**2001–2011.
4. **Bennett, J., S. P. Dretler, J. Selengut, and W. H. Orme-Johnson.** 1994. Identification of the calcium-binding protein calgranulin in the matrix of struvite stones. J. Endourol. **8:**95–98.
5. **Bichler, K. H., E. Eipper, K. Naber, V. Braun, R. Zimmermann, and S. Lahme.** 2002. Urinary infection stones. Int. J. Antimicrob. Agents **19:**488–498.
6. **Bouchelouche, K., S. Alvarez, T. Horn, J. Nordling, and P. Bouchelouche.** 2006. Human detrusor smooth muscle cells release interleukin-6, interleukin-8, and RANTES in response to proinflammatory cytokines interleukin-1β and tumor necrosis factor-alpha. Urology **67:**214–219.
7. **Chilosi, M., A. Mombello, L. Montagna, A. Benedetti, M. Lestani, G. Semenzato, and F. Menestrina.** 1990. Multimarker immunohistochemical staining of calgranulins, chloroacetate esterase, and S100 for simultaneous demonstration of inflammatory cells on paraffin sections. J. Histochem. Cytochem. **38:**1669–1675.
8. **Grenabo, L., J. E. Brorson, H. Hedelin, and S. Pettersson.** 1985. Concrement formation in the urinary bladder in rats inoculated with *Ureaplasma urealyticum*. Urol. Res. **13:**195–198.
9. **Healy, K. A., and K. Ogan.** 2007. Pathophysiology and management of infectious staghorn calculi. Urol. Clin. N. Am. **34:**363–374.
10. **Hicks, R. M.** 1975. The mammalian urinary bladder: an accommodating organ. Biol. Rev. Camb. Philos. Soc. **50:**215–246.
11. **Kasama, T., Y. Miwa, T. Isozaki, T. Odai, M. Adachi, and S. L. Kunkel.** 2005. Neutrophil-derived cytokines: potential therapeutic targets in inflammation. Curr. Drug Targets Inflamm. Allergy **4:**273–279.
12. **Kersey, P. J., J. Duarte, A. Williams, Y. Karavidopoulou, E. Birney, and R. Apweiler.** 2004. The International Protein Index: an integrated database for proteomics experiments. Proteomics **4:**1985–1988.
13. **Kunimi, K., M. Maegawa, M. Kamada, S. Yamamoto, T. Yasui, T. Matsuzaki, A. Kuwahara, H. Furumoto, Y. Ohmoto, H. Kido, and M. Irahara.** 2006. Myeloid-related protein-8/14 is associated with proinflammatory cytokines in cervical mucus. J. Reprod. Immunol. **71:**3–11.
14. **Mulvey, M. A., J. D. Schilling, J. J. Martinez, and S. J. Hultgren.** 2000. Bad bugs and beleaguered bladders: interplay between uropathogenic *Escherichia coli* and innate host defenses. Proc. Natl. Acad. Sci. USA **97:**8829–8835.
15. **Nacken, W., J. Roth, C. Sorg, and C. Kerkhoff.** 2003. S100A9/S100A8: myeloid representatives of the S100 protein family as prominent players in innate immunity. Microsc. Res. Tech. **60:**569–580.
16. **Nagata, K., E. Takagi, H. Satoh, H. Okamura, and T. Tamura.** 1995. Growth inhibition of *Ureaplasma urealyticum* by the proton pump inhibitor lansoprazole: direct attribution to inhibition by lansoprazole of urease activity and urea-induced ATP synthesis in *U. urealyticum*. Antimicrob. Agents Chemother. **39:**2187–2192.
17. **Parmar, M. S., K. H. Bichler, E. Eipper, K. Naber, V. Braun, R. Zimmermann, and S. Lahme.** 2004. Kidney stones. BMJ **328:**1420–1424.
18. **Pouliot, P., I. Plante, M. A. Raquil, P. A. Tessier, and M. Olivier.** 2008. Myeloid-related proteins rapidly modulate macrophage nitric oxide production during innate immune response. J. Immunol. **181:**3595–3601.
19. **Rahimi, F., K. Hsu, Y. Endoh, and C. L. Geczy.** 2005. FGF-2, IL-1β and TGF-β regulate fibroblast expression of S100A8. FEBS J. **272:**2811–2827.
20. **Reyes, L., M. Reinhard, and M. B. Brown.** 2009. Different inflammatory responses are associated with *Ureaplasma parvum*-induced UTI and urolith formation. BMC Infect. Dis. **9:**9.
21. **Reyes, L., M. Reinhard, L. J. O'Donell, J. Stevens, and M. B. Brown.** 2006. Rat strains differ in susceptibility to *Ureaplasma parvum*-induced urinary tract infection and struvite stone formation. Infect. Immun. **74:**6656–6664.
22. **Ryckman, C., K. Vandal, P. Rouleau, M. Talbot, and P. A. Tessier.** 2003. Proinflammatory activities of S100: proteins S100A8, S100A9, and S100A8/A9 induce neutrophil chemotaxis and adhesion. J. Immunol. **170:**3233–3242.
23. **Shilov, I. V., S. L. Seymour, A. A. Patel, A. Loboda, W. H. Tang, S. P. Keating, C. L. Hunter, L. M. Nuwaysir, and D. A. Schaeffer.** 2007. The Paragon Algorithm, a next generation search engine that uses sequence temperature values and feature probabilities to identify peptides from tandem mass spectra. Mol. Cell. Proteomics **6:**1638–1655.
24. **Smith, D. G., W. C. Russell, W. J. Ingledew, and D. Thirkell.** 1993. Hydrolysis of urea by *Ureaplasma urealyticum* generates a transmembrane potential with resultant ATP synthesis. J. Bacteriol. **175:**3253–3258.
25. **Staack, A., S. W. Hayward, L. S. Baskin, and G. R. Cunha.** 2005. Molecular, cellular and developmental biology of urothelium as a basis of bladder regeneration. Differentiation **73:**121–133.
26. **Stancombe, B. B., W. F. Walsh, S. Derdak, P. Dixon, and D. Hensley.** 1993. Induction of human neonatal pulmonary fibroblast cytokines by hyperoxia and *Ureaplasma urealyticum*. Clin. Infect. Dis. **17**(Suppl. 1)**:**S154–S157.
27. **Stone, K. L., and K. R. Williams.** 1997. Digestion of proteins in gels for sequence analysis, p. 11.3.1–11.3.12. *In* J. E. Coligan, B. M. Dunn, H. L. Ploegh, D. W. Speicher, and P. T. Wingfield (ed.), Current protocols in protein science, vol. 2. Wiley & Sons, Inc., Hoboken, NJ.
28. **Striz, I., and I. Trebichavsky.** 2004. Calprotectin—a pleiotropic molecule in acute and chronic inflammation. Physiol. Res. **53:**245–253.
29. **Tolson, J. P., T. Flad, V. Gnau, H. Dihazi, J. Hennenlotter, A. Beck, G. A.**

Mueller, M. Kuczyk, and C. A. Mueller. 2006. Differential detection of S100A8 in transitional cell carcinoma of the bladder by pair wise tissue proteomic and immunohistochemical analysis. Proteomics **6:**697–708.
30. **Tyagi, P., X. Chen, Y. Hayashi, N. Yoshimura, M. B. Chancellor, and F. de Miguel.** 2008. Proteomic investigation on chronic bladder irritation in the rat. Urology **71:**536–540.
31. **Viemann, D., K. Barczyk, T. Vogl, U. Fischer, C. Sunderkotter, K. Schulze-Osthoff, and J. Roth.** 2007. MRP8/MRP14 impairs endothelial integrity and induces a caspase-dependent and -independent cell death program. Blood **109:**2453–2460.
32. **Viemann, D., A. Strey, A. Janning, K. Jurk, K. Klimmek, T. Vogl, K. Hirono, F. Ichida, D. Foell, B. Kehrel, V. Gerke, C. Sorg, and J. Roth.** 2005. Myeloid-related proteins 8 and 14 induce a specific inflammatory response in human microvascular endothelial cells. Blood **105:**2955–2962.
33. **Whiteland, J. L., C. Shimeld, S. M. Nicholls, D. L. Easty, N. A. Williams, and T. J. Hill.** 1997. Immunohistochemical detection of cytokines in paraffin-embedded mouse tissues. J. Immunol. Methods **210:**103–108.
34. **Yui, S., Y. Nakatani, and M. Mikami.** 2003. Calprotectin (S100A8/S100A9), an inflammatory protein complex from neutrophils with a broad apoptosis-inducing activity. Biol. Pharm. Bull. **26:**753–760.

Editor: R. P. Morrison